JMEPEG (2019) 28:2779–2787
https://doi.org/10.1007/s11665-019-04094-z

1059-9495/$19.00

Effect of Forging on Microstructure, Mechanical Properties and Acoustic Emission Characteristics of Al Alloy (2014): 10 wt.% SiC_p Composite

Amulya Bihari Pattnaik, Satyabrat Das, and Bharat Bhushan Jha

(Submitted September 4, 2018; in revised form April 25, 2019; published online May 10, 2019)

In this paper a systematic study has been undertaken to study the effect of forging on microstructure, mechanical properties and acoustic emission (AE) characteristics of Al alloy (2014)—10 wt.% SiC metal-matrix composites. Hammer forging was carried out at a temperature of 470 °C in an open die, with a deformation ratio of 3.5:1. Microstructural analyses were carried out at three different positions of forged billet. Significant material flow was observed in the sample taken from the sides of the forged billet, but no appreciable material flow was observed at the center of the forged billet. The microstructural characterization showed that forging resulted in cracking of SiC particles in Al alloy (2014)—10 wt.% SiC composite. The AE results during forging showed an increase in AE signal intensity during the initial yielding period and a subsequent decrease in the intensity of AE signals with sudden burst at the end of the forging. The plastic deformation at room temperature was less ductile in nature but at high temperature, appreciable ductility was observed. The FESEM micrographs of fracture surfaces of the tensile specimens showed appreciable clustering of SiC particles during plastic deformation both at room and high temperature.

Keywords acoustic emission, debonding, deformation, field emission scanning electron microscopy (FESEM), interface, metal-matrix composites (MMCs)

1. Introduction

Aluminum-based metal-matrix composites (AMCs) have superior properties compared to that of conventional alloys such as improved specific strength and stiffness, good wear resistance and improved high-temperature properties for which it has received great attention (Ref 1). The improved mechanical properties, low manufacturing cost and ease of fabrication make the AMCs a potential structural material for automotive and aerospace applications. These characteristics of AMCs make them an important material to substitute steels and cast iron in major engineering applications (Ref 2). These composites are manufactured by conventional casting techniques like stir casting due to low cost and simple process. Mechanical working of AMCs by forging, extrusion or rolling to obtain a final shape needs a thorough understanding of deformation behavior. Numerous investigations have been carried out to study the deformation behavior of AMCs (Ref 3-10). Some of the previous work on mechanical working in metals showed improved properties due to grain refinement, uniform particle distribution and strong interfacial bonding (Ref 11-17). Ceschini et al. (Ref 18, 19) during their investigation on forging of AA2618/20 vol.% Al_2O_{3p} and AA6061/23 vol.% Al_2O_{3p} composite showed that forging results in reduced porosity and lesser damage in the forged billet mainly due to high temperature and low deformation ratio. They also showed that forging resulted in increase in tensile strength and elongation both at room and high temperature. Wu et al. (Ref 20) systematically studied the effect of forging on microstructure and mechanical properties of SiC/AZ91 magnesium matrix composite. They showed that the yield and the ultimate tensile strength of the composite increase due to forging. Shi et al. (Ref 21) during their investigation of forged 2024Al/$Al_{18}B_4O_{33}$w composite found large differences in distribution of reinforcement in the forged composite. They also found that forging leads to increased ductility at room as well as at high temperature. Most of the investigations on secondary processing of AMCs reported so far are on extrusion behavior of AMCs, while very few studies have been carried out to study the effect of forging (Ref 14, 16, 18, 19).

Acoustic emissions (AE) are transient elastic waves generated from within the material due to the dynamic events occurring inside the material due to application of load (Ref 22). Real-time information is obtained by online monitoring of deformation process (Ref 23). Acoustic emission studies have been used to obtain real-time information for variety of metal-working processes including forging (Ref 24). AE has been used to monitor various deformation phenomena like crack initiation and propagation (Ref 25).

The present study aims to evaluate the effect of forging on microstructure, mechanical properties and acoustic emission characteristics of Al alloy (2014)—10 wt.% SiC composite. The main aim is to study the material flow behavior in the AMC due to hot forging. The tensile properties of the forged billet were compared with the fracture surface to evaluate the damage mechanism responsible for failure. The acoustic emission technique was used to correlate the AE signal

Amulya Bihari Pattnaik, Indira Gandhi Institute of Technology (IGIT), Sarang, Dhenkanal, Odisha, India; **Satyabrat Das**, CSIR-Advanced Materials and Processes Research Institute (AMPRI), Bhopal, India; and **Bharat Bhushan Jha**, CSIR-Central Glass and Ceramic Research Institute (CGCRI), Kolkata, India. Contact e-mails: amulyapattnaik@gmail.com and amulyapattnaik@igitsarang.ac.in.

parameters with the microstructure and deformation of the forged sample.

2. Experimental

2.1 Materials and Microstructure

In the present investigation an aluminum alloy AA2014 matrix reinforced with 10 wt.% of SiC particles was used. The AA2014 alloy generally contains 4.5 wt.% Cu, 0.97 wt.% Mg, 0.8 wt.% Fe and balance aluminum. The composite was prepared by stir casting process. The process involves (1) melting of AA2014 alloy in a graphite crucible in an electrical resistance furnace, (2) dispersion of preheated 10 wt.% SiC particles (size 20-40 μm) in the melt followed by mechanical stirring, (3) casting and solidification of melt in the form of billet (120 mm diameter and 250 mm height). The billet was homogenized at 450 °C for 16 h before forging. The as-cast billet was hammer forged at 470 °C in an open die using a graphite-based lubricant. The forging parameters and the schematic of forging process are given in Table 1 and Fig. 1, respectively. The microstructural examinations were carried out in a field emission scanning electron microscope (NOVA NANO FESEM 430). The samples for microstructural characterization were taken from three different positions as shown in Fig. 1. The forged billet was cut into two halves and samples were cut in a direction perpendicular to the direction of forging.

Table 1 Forging parameters

Initial diameter of billet, mm	120
Initial height of billet, mm	250
Final height of billet, mm	70
Deformation ratio	3.5:1
Temperature of forging	470 °C

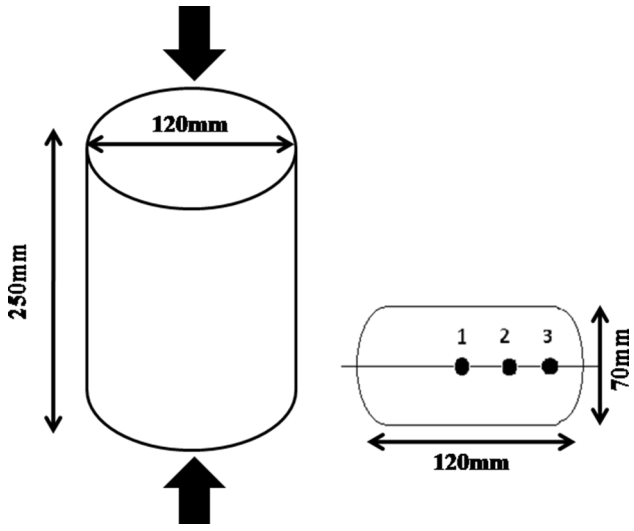

Fig. 1 Schematic of forged AA2014—10 wt.% SiC composite

The samples were polished using conventional metallographic techniques and etched with Keller's reagent to study the material flow behavior.

2.2 Measurement of Elastic Modulus

The Young's modulus or elastic modulus of the forged AA2014—10 wt.% SiC composite was measured using dynamic elastic property analyzer (DEPA). It is an advanced system for testing the elastic properties of materials using impulse excitation technique (IET). Samples of dimension 60.01 mm × 30.20 mm × 5.64 mm were used for the analyses. During testing the samples were excited using an impulse tool. The natural frequency was detected and used for measurement of elastic modulus. The average value of five readings was reported.

2.3 Hardness

The Brinell hardness values of polished samples were taken from three different position of forged billet was measured using a Universal hardness tester with a load of 62.5 N. The average values of five readings for each sample were reported.

2.4 X-ray Diffraction Studies

The x-ray diffraction studies were performed on forged Al 2014—10% SiC composite to identify different phases present. The diffraction carried out at a scanning speed of 2°/min with a CuK_{α} (λ = 1.54 Å) x-ray. The x-ray diffraction (XRD) plot with various phases present is shown in Fig. 2.

2.5 Mechanical Characterization

Cylindrical tensile specimens of dimensions of 20 mm diameter, 8-mm-gauge width and 40-mm-gauge length were cut from the forged billet with tensile axis perpendicular to the forging direction. Both room and high-temperature tensile tests were carried out on a floor model INSTRON 8801 servo hydraulic universal testing machine of 100 kN capacity. The

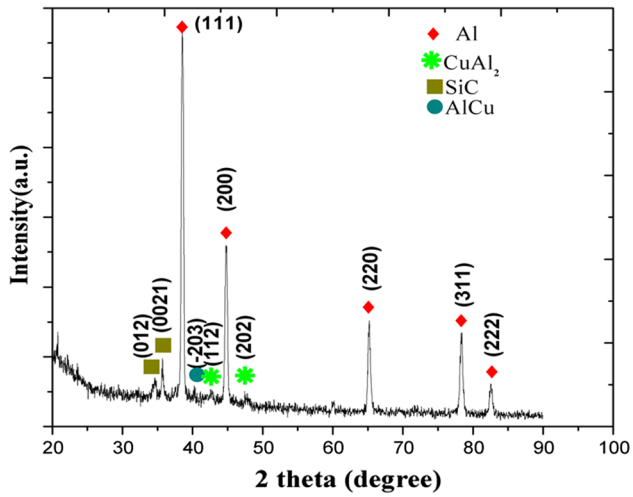

Fig. 2 XRD plot showing the various phases present in forged Al 2014—10% SiC composite

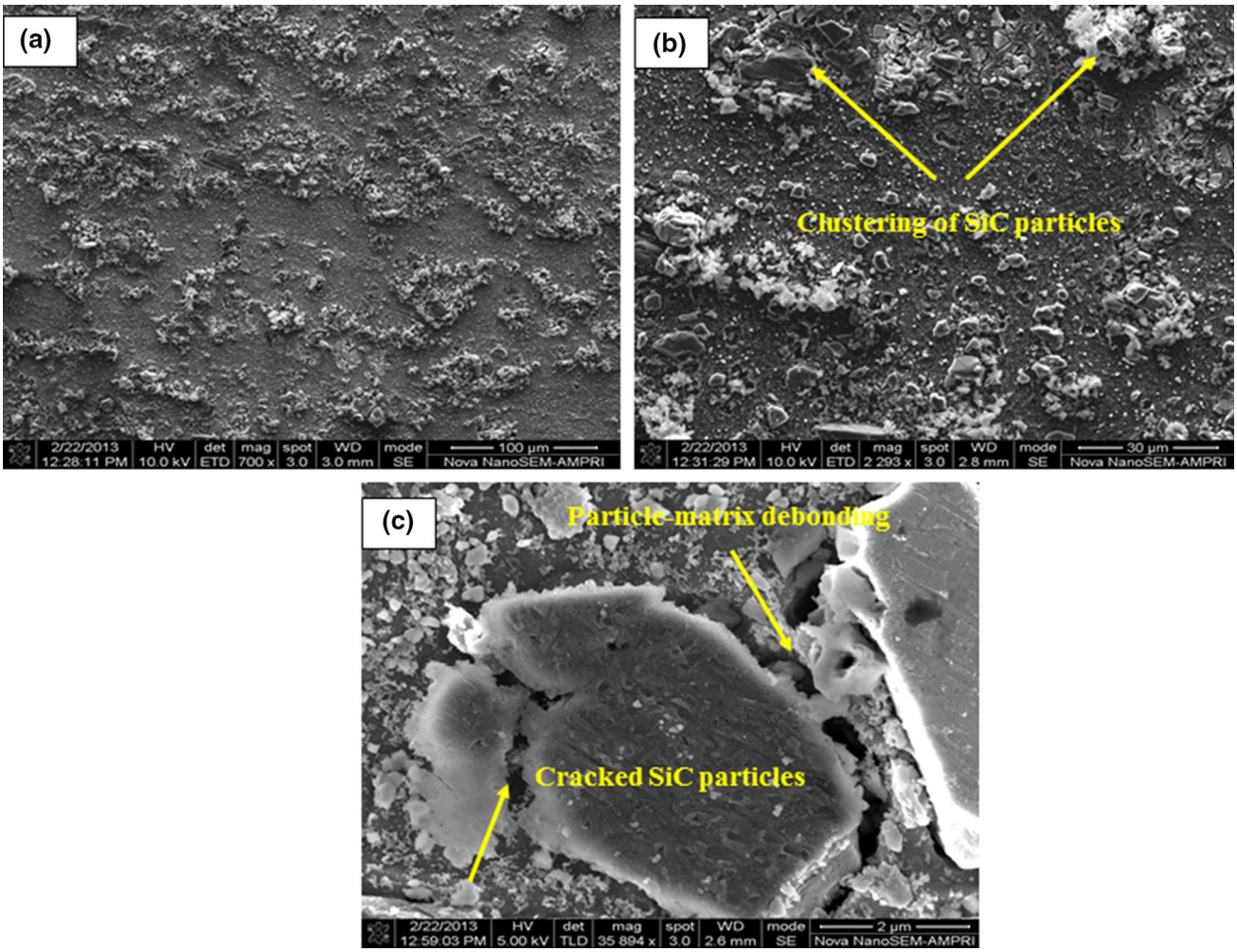

Fig. 3 FESEM micrograph of the sample taken from (a) position 1, i.e., from the center of the forged billet (b) position 1, i.e., from the center of the forged billet showing clustering of SiC particles. (c) Higher magnification micrograph of the sample taken from the center of the forged billet (i.e., position 1)

tests were carried out at a strain rate of 10^{-2} s^{-1}. Impact test of the forged AA2014—10 wt.% SiC composite was carried out in an INSTRON make impact testing machine. Charpy V-notch impact specimens with dimension 10 mm × 10 mm × 55 mm were prepared according to ASTM A370 (Ref 26). The damage mechanisms during plastic deformation were studied using FESEM analysis of fracture surfaces.

2.6 Acoustic Emission Testing

Acoustic emission testing during forging was carried out using a two-channel PCI-DiSP with an AEwin version E2.32 AE system (Physical Acoustic Corporation, Princeton, NJ, USA). AE signals were detected using a resonant transducer of peak frequency 150 kHz. The AE sensor was placed on the bottom die of the forging press. This is the optimum position to mount the AE sensor which is well documented in the literature (Ref 27). A preamplifier with a gain of 40 dB and a compatible filter (10 kHz-2 MHz) were used to capture the AE signals. By using the Kaiser effect, a threshold was set with 45 dB to avoid the background noise. A total gain of 100 dB was used to capture the AE signals.

3. Results and Discussion

3.1 Effect of Forging on Microstructure

Field emission scanning electron micrographs (FESEM) were taken at three different positions of the forged billet (according to Fig. 1) to study the material flow behavior due to forging. Figure 1 shows that position 1 is the center of the forged billet, while positions 2 and 3 are the sides of the forged billet. Figure 3(a) shows the FESEM micrograph of the sample taken from position 1, i.e., from the center of the forged billet. From the figure, it is clearly observed that grains of primary alpha Al are elongated in a direction perpendicular to the forging and SiC particles are distributed in the alloy matrix. However, no significant localized grain flow was observed at the center of the forged billet. Clustering or agglomeration of SiC particles is clearly evident from Fig. 3(b) (position 1). This may be attributed to high localized deformation at the center of the forged billet. Figure 3(c) shows the higher magnification micrograph of the sample taken from the center of the forged billet (i.e., position 1) clearly depicting the particle–matrix

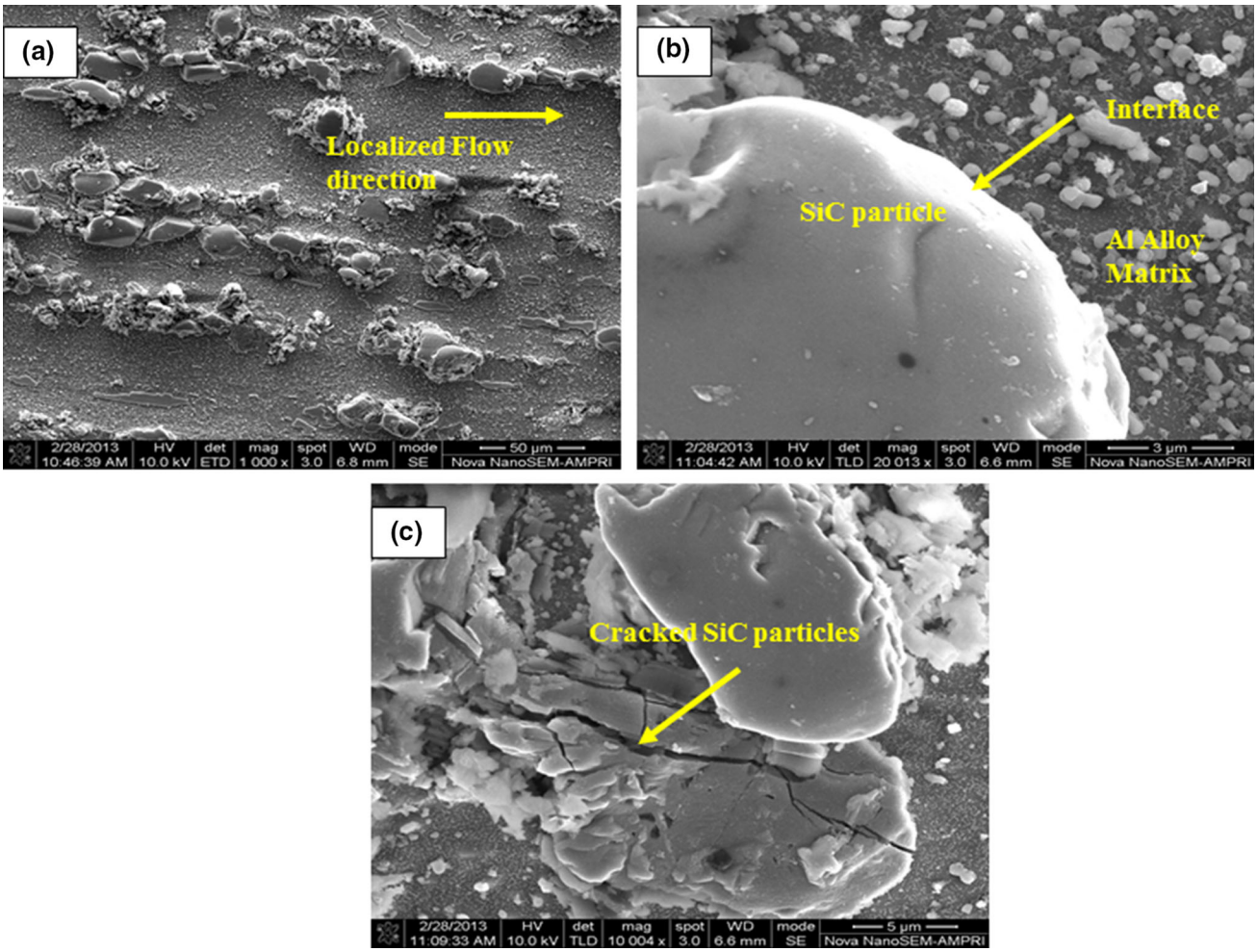

Fig. 4 FESEM micrograph of the sample taken from (a) position 2 of the forged billet showing localized grain flow (b) position 2 of the forged billet depicts the interfacial bonding (higher magnification) (c) position 2 of the forged billet showing cracking of the reinforcing particles (higher magnification)

debonding and fracture/cracking of SiC particles. This can be attributed to severe stress concentration on the SiC particles during the process of load transfer from ductile Al alloy matrix to brittle SiC particles. In composites, the overall deformation behavior is controlled by the matrix–particle interface because the transfer of load from alloy to particles has a profound effect on the interface. Figure 4(a) shows the micrograph of the sample taken from position 2 (Fig. 1) of the forged billet. From the figure, significant localized grain flow was observed. Primary Al alpha grains and SiC particles are elongated in a direction perpendicular to forging. Clustering of SiC particles was found to be less in position 2 as compared to position 1. This is mainly due to the localized flow of individual SiC particles. Figure 4(b) shows the higher magnification micrograph of the sample taken from position 2 of the forged billet clearly depicting the interfacial bonding. The combined flow of Al alloy matrix and SiC particles results in reduced particle–matrix debonding. Cracking of the SiC particles was also observed in position 2 of the forged billet (Fig. 4c). This is mainly attributed to the stress concentration on the SiC particles during load transfer from matrix to particles.

Figure 5(a) shows the micrograph of the sample taken from position 3, i.e., from the sides of the forged billet. Much more significant localized grain flow was observed in position 3 in comparison with position 2. Al alloy matrix along with SiC particles flew in a direction perpendicular to forging. Figure 5(b) shows the higher magnification micrograph of the sample taken from position 3 of the forged billet clearly indicating strong matrix–particle bonding at the interface. This is mainly attributed to lesser stress concentration at the interface which is mainly due to localized flow of grains. Due to lesser stress concentration particle cracking was found to be significantly less (Fig. 5c). The flow of Al matrix and $CuAl_2$ precipitate is shown in Fig. 6. It is clearly observed that the precipitates flow along the grain boundaries.

3.2 Effect of Forging on Mechanical Properties

3.2.1 Hardness Tests. Brinell hardness of the samples taken from different position (Fig. 1) of the forged composite was measured. The hardness values were found to be

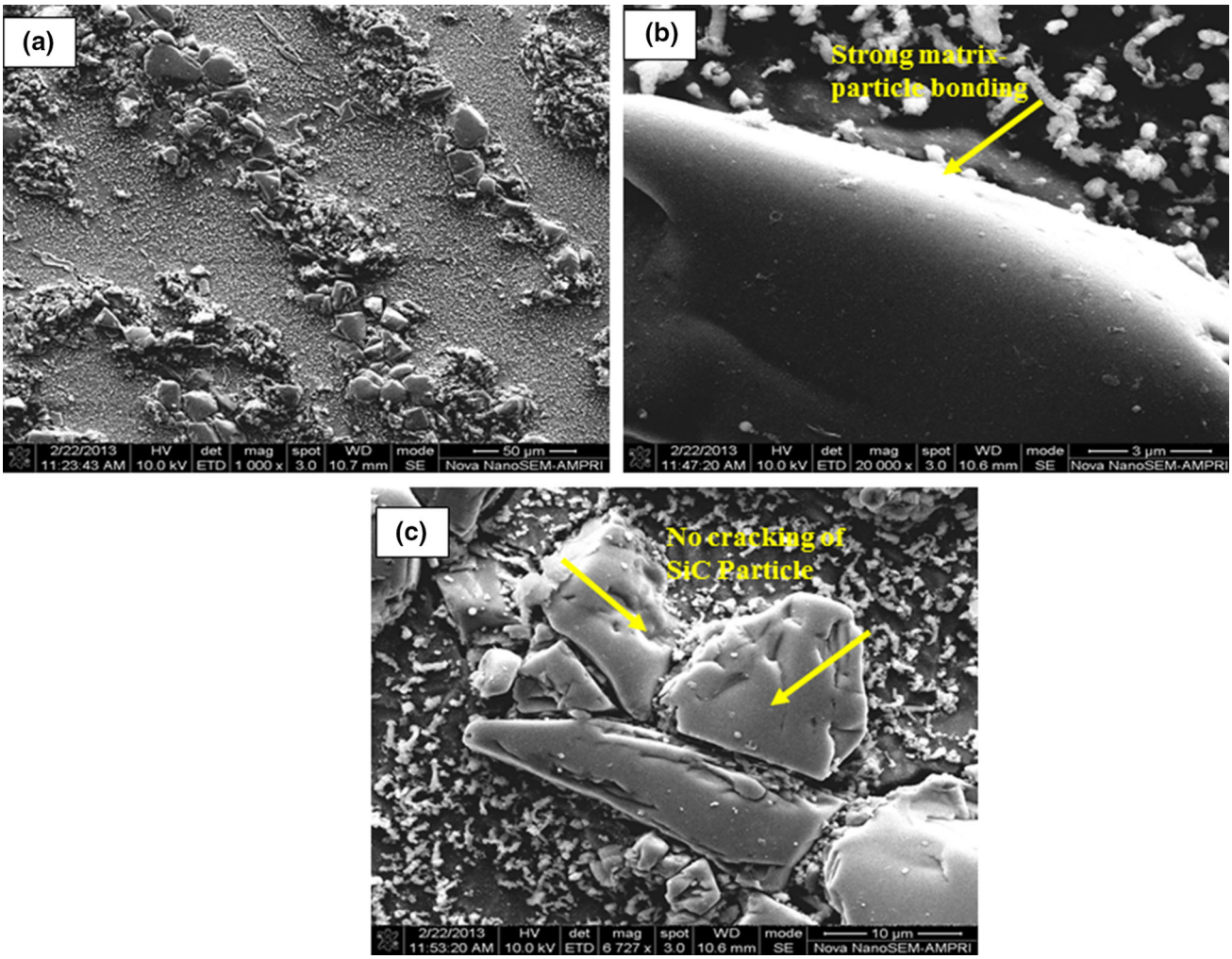

Fig. 5 FESEM micrograph of the sample taken from (a) position 3, i.e., sides of the forged billet (b) position 3 of the forged billet clearly indicating strong matrix–particle bonding at the interface (higher magnification) (c) position 3 of the forged billet showing no cracking of reinforcing particles (higher magnification)

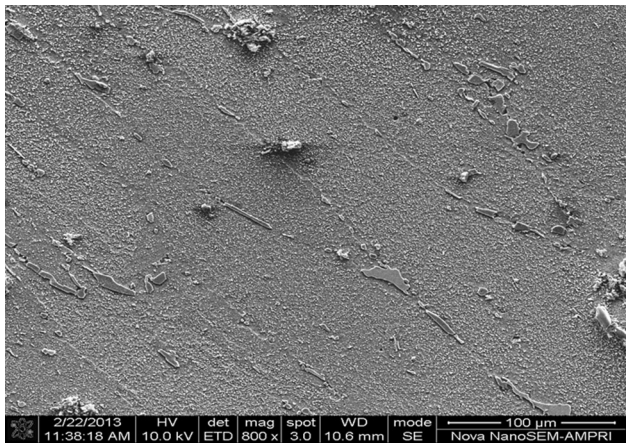

Fig. 6 FESEM micrograph of forged billet depicting the flow of Al matrix and precipitates

(64.20 ± 0.5) BHN, (60.3 ± 0.5) BHN and (56.7 ± 0.5) BHN for position 1, position 2 and position 3, respectively, of the forged billet. The hardness value was found to be higher at the center (position 1) of the forged billet which is mainly attributed to highly localized deformation and clustering of SiC particles. However, the hardness value decreased as we move from position 2 to position 3 owing particularly to the high flow ability of Al matrix and SiC particles.

3.2.2 Tensile and Impact Tests. The results of the tensile tests carried out at room and high temperature are given in Table 2 and Fig. 7. The elastic modulus of the forged composite was measured using Dynamic Elastic Property Analysis (DEPA) and was found to be 65 GPa. The lower value of elastic modulus is mainly associated with matrix–particle decohesion and cracking of the particles during forging, which decreases the strength of the interface.

In author's previous work (Ref 28, 29), on the study of hot deformation behavior of AA2014—10 wt.% SiC composite using compression, the yield stress at room temperature and 300 °C was found to be 300 and 100 MPa, respectively. The lower values of yield stress in the present work are mainly attributed to the more localized compressive deformation during hammer forging resulting in cracking of brittle SiC particles. Moreover, the formation of brittle intermetallic compounds (Fig. 10) weakens the particle–matrix interface.

Table 2 Tensile tests results for forged composite and AA 2014 as-cast without SiC tested at room and high temperature

Material	Temperature, °C	Yield strength, MPa(0.2% offset)	Ultimate tensile strength, MPa	Total elongation, %
AA 2014 forged	Room temperature	71.58 ± 9	170.39 ± 14	10 ± 0.5
	300	69.23 ± 10	142.65 ± 9	17 ± 0.5
Forged composite	Room temperature	74.22 ± 11	157.22 ± 12	7 ± 0.5
	300	124.62 ± 9	139.97 ± 10	14 ± 0.5

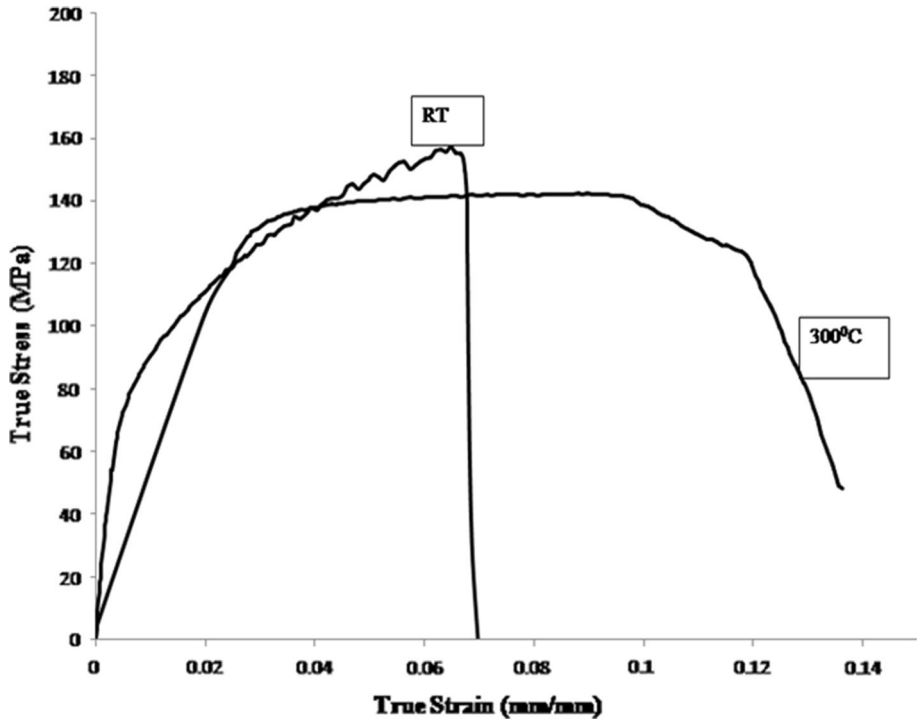

Fig. 7 True stress–true strain curves for forged composite tensile tested at room and high temperature (300 °C)

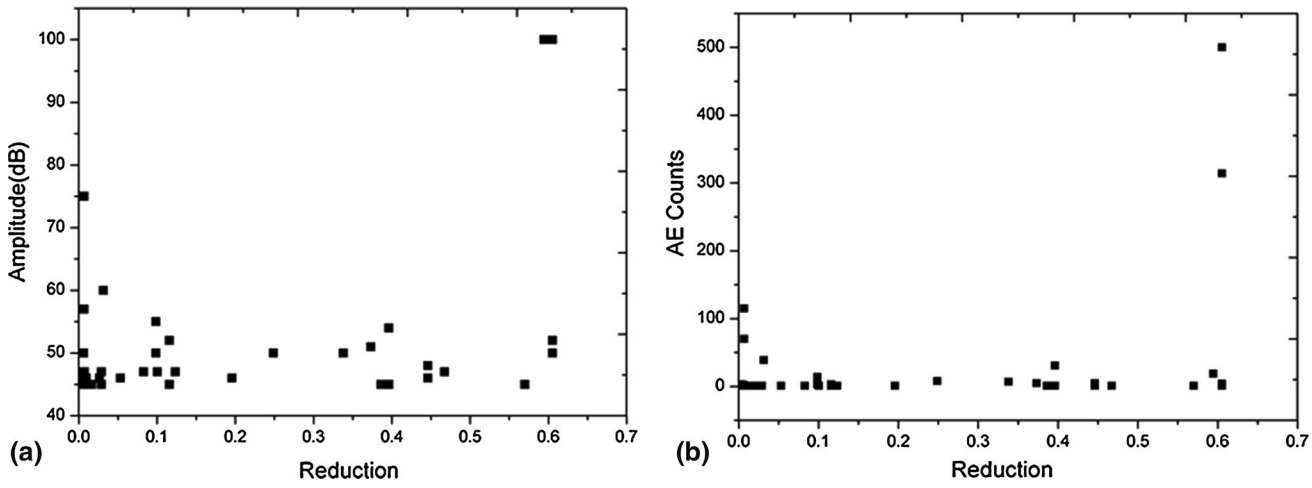

Fig. 8 (a) Variation of AE counts and (b) AE amplitude with the reduction during forging of the composite

The forging of AA2014—10 wt.% SiC composite resulted in an increase in yield and ultimate tensile strength both at room and high temperature (Table 2) as compared to the AA2014 forged alloy without SiC. This is mainly attributed to the localized grain flow during forging which resulted in declustering of SiC particles. A similar observation was reported for other MMCs (Ref 11, 30) after forging. The increase in strength of the composite after forging is mainly attributed to the grain refinement and reduction in porosity (Ref 31-33). The grain size was calculated using image analysis software ImageJ and was found to be 140 μm for as-cast composite and 91 μm for forged composite. The increase in the yield strength at high temperature (300 °C) can be attributed to the stability of the Al2014 matrix (Ref 34). The forging of AA2014—10 wt.% SiC

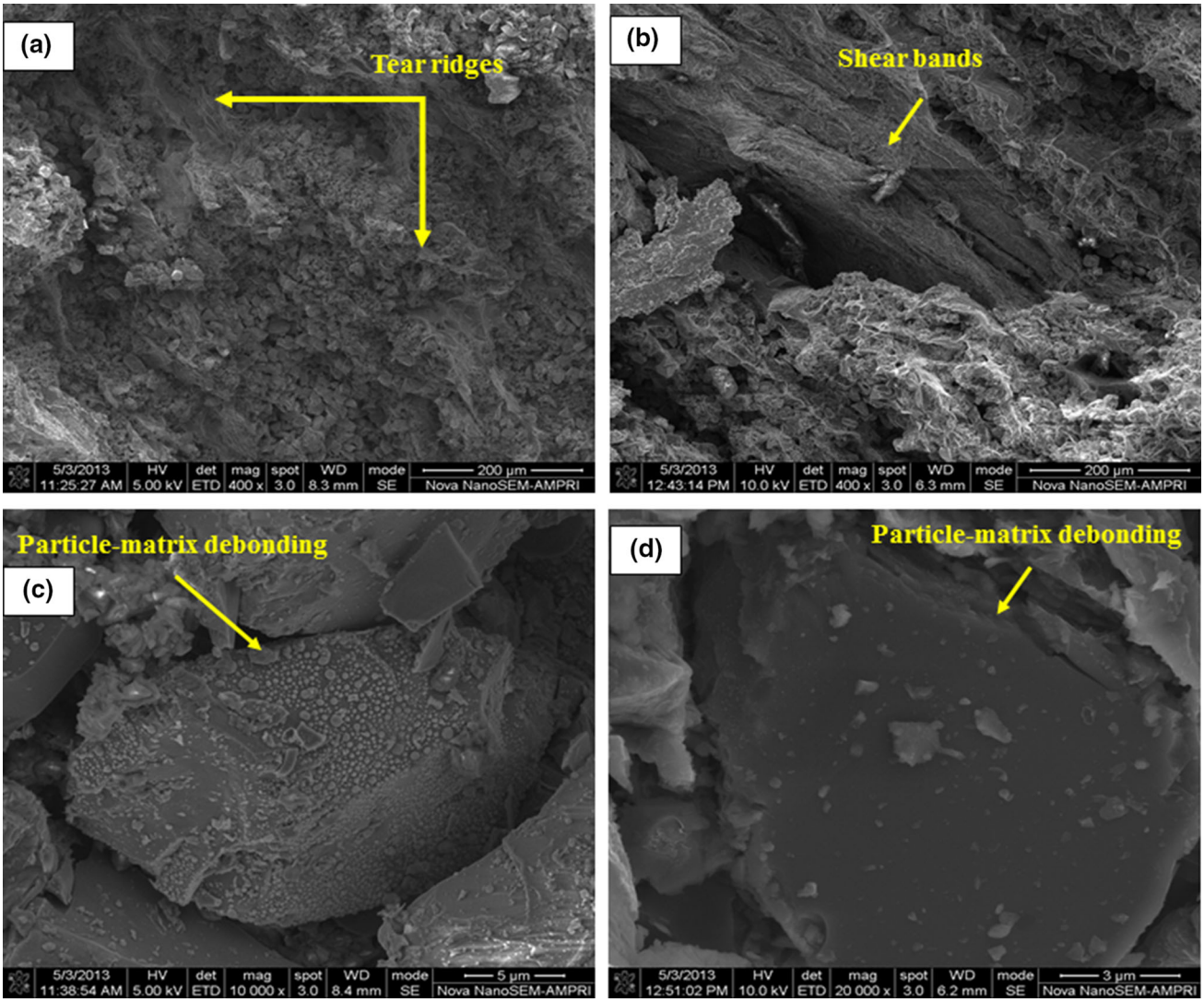

Fig. 9 FESEM micrographs of the fracture surfaces of forged composite tested at (a) room temperature and (b) 300 °C at (c) room and (d) high temperature (300 °C) clearly depicting the debonding between the particle and matrix (higher magnification)

composite increases its elongation to fracture, i.e., ductility. The ductility was found to be twice at room temperature and thrice at high temperature as compared to as-cast composite (Ref 35). From Fig. 7, it is observed that for the sample tested at 300 °C, the ductility was found to be considerably higher (14%) which can be attributed to the microstructural modification due to grain refinement and porosity reduction. The improved ductility at high temperature can also be attributed to recovery and recrystallization taking place in the matrix. The impact test of both as-cast and forged composite was carried out using a motorized impact tester. The average of five readings was taken and found to be 1.05 and 0.986 J, respectively. The lower value of impact energy for forged composite signifies brittle failure which can be attributed to triaxial state of stress existing at the notch, low temperature and high rate of loading.

3.3 Effect of Forging on Acoustic Emission Characteristics

Figure 8(a) and (b) shows the variation of AE counts and AE amplitude with the reduction during forging of the composite. It is clearly observed from the figure that the forging process is divided into three regions (1) Initial yielding during upsetting (2) Intermediate region of deformation (3) Increase in contact area and friction due to die filling. A peak is observed in both AE counts and amplitude during the initial yielding which is mainly attributed to the fracture/cracking of SiC particles at the center. This may be due to highly localized deformation at the center. After 9-10% of deformation, it is observed that the AE signal intensity decreases. This may be attributed to the completion of fracture/cracking of SiC particles. The decrease in AE intensity is also attributed to dynamic recovery, which is the dominant softening mechanism in high stacking fault energy material like aluminum. The dynamic recovery leads to low dislocation densities due to ease of cross slip, climb and dislocation unpinning at nodes. Beyond 40% of deformation, friction between the workpiece and the die dominates the AE signal profile. Increase in deformation results in increase in the contact area due to the die filling. The sudden burst in the AE signal at 60% deformation is mainly due to the combined effect of particle–matrix debonding and the frictional forces between the material and die interface. This is well correlated with the forged microstructure.

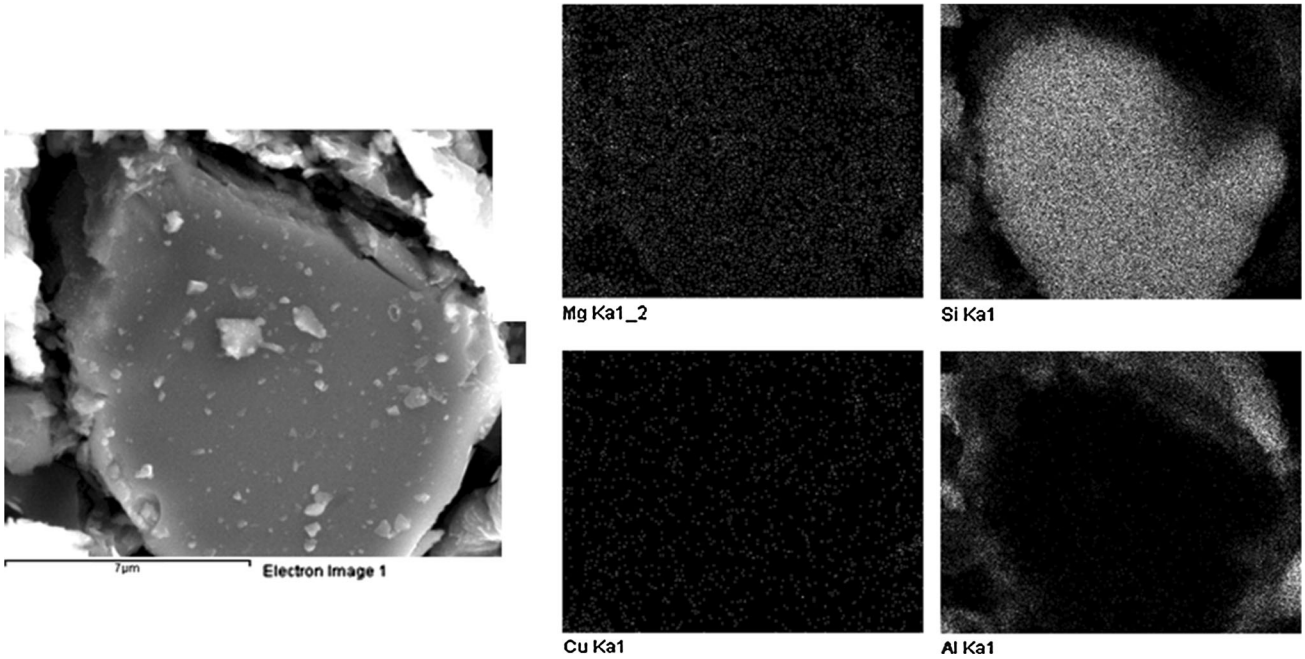

Fig. 10 EDS maps of the SiC particle for the sample tensile tested at 300 °C showing the elemental distribution of Mg, Cu, Si, Al

4. Fracture Surfaces

Figure 9(a) and (b) shows the fracture surfaces of the forged composite tensile tested at room and high temperatures. From the figure, it is clearly observed that fracture surface at room temperature test (Fig. 9a) is associated with formation of large voids, fine dimples or tear ridges and particle–matrix debonding which is in accordance with some of the previous studies (Ref 36). The debonding mainly occurs due to high stress concentration at the interface. Clustering of SiC particles was observed at room temperature. At higher temperature (300 °C), the failure is mainly ductile in nature as evident from Fig. 9(b). The increase in ductility may be due to over aging of the matrix phase. A large number of micro-voids with dimples and particle–matrix debonding were observed from the fracture surface. The formation of shear bands is also clearly observed from the figure. The fracture occurs due to the stress concentration on these shear bands. Matrix cracking was also observed.

Figure 9(c) and (d) shows the higher magnification micrograph of fracture surfaces of forged composite tensile tested at room and high temperatures clearly depicting the debonding between the particle and matrix. Cracking of SiC particles was observed in Fig. 9(a) and (b). This is mainly due to higher localized stress concentration. The failure occurs owing particularly to the particle matrix debonding. Figure 10 shows the energy dispersive spectroscopy (EDS) maps of the SiC particle and the particle matrix interface for the sample tensile tested at 300 °C. It showed that the interface is rich in Mg and Cu. This results in the formation of brittle intermetallic compounds which has been detected in XRD peaks in Fig. 2. The presence of these intermetallic compounds weakens the particle–matrix interface and reduces the load transfer capability from the matrix phase to the reinforcing phase contributing to particle/matrix debonding.

5. Conclusions

The following conclusions were drawn from the above study:

1. The microstructural characterization of the forged composite showed that no significant material flow was observed at the center of the forged billet. However, significant flow of Al alloy matrix and SiC particles was observed at the sides of the forged billet.
2. Forging resulted in an increase in tensile strength and elongation to failure in the forged composite both at room and high temperatures.
3. The AE activity during forging is divided into three regions (1) Initial yielding during upsetting (2) Intermediate region of deformation (3) Increase in contact area and friction due to die filling. The sudden burst at the end of the deformation is attributed to the combined effect of particle–matrix debonding and friction due to die filling.
4. Fracture surfaces of forged composite at room and high temperatures were mainly characterized by ductile failure of the matrix and particle–matrix debonding which occurs due to the presence of brittle compounds.

Acknowledgments

The Authors would like to thank The Director, Indira Gandhi Institute of Technology, Sarang, Odisha, India, for his constant

encouragement and support. The authors would also like to acknowledge the financial support of the Council of Scientific and Industrial Research under the Project ESC-0101.

References

1. D.P. Mondal, S. Das, K.S. Suresh, and N. Ramakrishnan, Compressive Deformation Behaviour of Coarse SiC Particle Reinforced Composite: Effect of Age Hardening and SiC Content, *Mater. Sci. Eng. A*, 2007, **460-461**, p 550–560
2. A. Patel, S. Das, and B.K. Prasad, Compressive Deformation Behaviour of Al Alloy (2014)—10 wt.% SiC_p Composite: Effects of Strain Rates and Temperatures, *Mater. Sci. Eng. A*, 2011, **530**, p 225–232
3. T.S. Srivatsan, M. Al-Hajiri, C. Smith, and M. Petraroli, The Tensile Response and Fracture Behaviour of 2009 Aluminium Alloy Metal Matrix Composite, *Mater. Sci. Eng. A*, 2003, **346**, p 91–100
4. D.L. McDanels, Analysis of Stress–Strain, Fracture and Ductility Behaviour of Aluminium Matrix Composites Containing Discontinuous Silicon Carbide Reinforcement, *Metall. Trans. A*, 1985, **16**(6), p 1105–1115
5. R.B. Grishaber, R.S. Mishra, and A.K. Mukhrjee, Effect of Testing Environment on Intergranular Microsuperplasticity in Aluminium MMC, *Mater. Sci. Eng. A*, 1996, **220**, p 78–84
6. T.G. Nieh, Creep Rupture of Silicon Carbide Reinforced Aluminium Composite, *Metall. Trans. A*, 1984, **15**(1), p 139–150
7. Y. Sugimura and S. Suresh, Effect of SiC Content on Fatigue Crack Growth in Aluminium Metal Matrix Composite, *Metall. Trans. A*, 1992, **23**, p 2231–2242
8. A.S. Argon, J. Im, and R. Safoglu, Cavity Formation in Inclusions from Ductile Fracture, *Metall. Trans. A*, 1975, **6**, p 825–831
9. T. Christman, A. Needleman, S. Nutt, and S. Suresh, On Microstructural Evolution and Micromechanical Modelling of Deformation of a Whisker Reinforced Metal Matrix Composite, *Mater. Sci. Eng. A*, 1989, **107**, p 49–59
10. M.P. Singh and J.J. Lewandowski, Effect of Heat Treatment and Reinforcement Size on Reinforcement Fracture During Tension Testing of a SiC Discontinuously Reinforced Aluminium Alloy, *Metall. Trans. A*, 1993, **24**, p 2531–2542
11. Y.H. Seo and C.G. Kang, Effect of Hot Extrusion Through a Curved Die on the Mechanical Properties of SiC_p Aluminium Composites Fabricated by Melt Stirring, *Compos. Sci. Technol.*, 1999, **59**(5), p 643–654
12. G.A. Rozak, A. Altmisoglu, J.J. Lewandowski, and J.F. Fallace, Effect of Casting Conditions and Deformation Processing on A356 Aluminium and A356 20 vol.% SiC Composites, *J. Compos. Mater.*, 1992, **26**, p 2076–2106
13. D. Zhao, F.R. Tuler, and D.J. Lloyd, Fracture at Elevated Temperature in a Particle Reinforced Composite, *Acta Metall. Sin. (Engl. Lett.)*, 1994, **42**(7), p 2525–2533
14. P. Cavaliere, Isothermal Forging of AA2618 reinForced with 20% of Alumina Particles, *Compos. Part A*, 2004, **35**(6), p 619–629
15. S.J. Barnes, P.B. Prangnell, S.M. Roberts, and P.J. Withers, The Influence of Temperature on Microstructural Damage During Uniaxial Compression of Aluminium Matrix Composites, *Scr. Mater.*, 1995, **33**(2), p 323–329
16. C. Badini, G.M. La Vecchia, P. Fino, and T. Valente, Forging of 2124/SiC_p Composite: Preliminary Studies of the Effects On Microstructure and Strength, *J. Mater. Process. Technol.*, 2001, **116**(2-3), p 289–297
17. A. Manna and B. Bhattacharya, A Study on Machinability of Al/SiC-MMC, *J. Mater. Process. Technol.*, 2003, **140**(1-3), p 711–716
18. L. Ceschini, G. Minak, A. Morri, and F. Tarterini, Forging of AA6061/23 vol.%Al_2O_3 Composite: Effect on Microstructure and Tensile Properties, *Mater. Sci. Eng. A*, 2009, **513-514**, p 176–184
19. L. Ceschini, G. Minak, and A. Morri, Forging of AA2618/20 vol.%Al_2O_3 Composite: Effect on Microstructure and Tensile Properties, *Compos. Sci. Technol.*, 2009, **69**, p 1783–1789
20. K. Wu, K. Deng, H. Chang, Y. Wu, X. Hu, and M. Zheng, Effect of Forging Temperature on Microstructure and Mechanical Properties of the SiC_p/AZ91 Magnesium Matrix Composite, *Acta Metall. Sin. Engl. Lett.*, 2010, **23**, p 99–105
21. W.C. Shi, L. Yuan, Z.Z. Zheng, and D.B. Shan, Effect of Forging on the Microstructure and Tensile Properties of 2024Al/$Al_{18}B_4O_{33}$w Composite, *Mater. Sci. Eng. A*, 2014, **615**, p 313–319
22. A.B. Pattnaik, S. Das, B.B. Jha, and N. Prasanth, Effect of Al-5Ti-1B Grain Refiner on the Microstructure, Mechanical Properties and Acoustic Emission Characteristics of Al5052 Aluminium Alloy, *J. Mater. Res. Technol.*, 2014, **4**, p 171–179
23. A.B. Pattnaik, B.B. Jha, and R. Sahoo, Effect of Strain Rate on Acoustic Emission During Tensile Deformation of α-Brass, *Mater. Sci. Technol.*, 2013, **29**(3), p 294–299
24. W.M. Mullins, R.D. Irwin, J.C. Malas, III, and S. Venugopal, Examination on the Use of Acoustic Emission for Monitoring Metal Forging Process: A Study Using Simulation Technique, *Scr. Mater.*, 1997, **36**(9), p 967–974
25. I. El-Galy and B.-A. Behrens, Online Monitoring of Hot Die Forging Processes Using Acoustic Emission (Part I), *J. Acoust. Emiss.*, 2008, **26**, p 208–219
26. ASTM A370-12, *Standard Test Methods and Definitions for Mechanical Testing of Steel Products* (ASTM International, West Conshohocken, PA, 2012). www.astm.org
27. C.K. Mukhopadhyay, S. Venugopal, T. Jayakumar, S.L. Mannan, B. Raj, B. Chatterji, R. Srinivasan, V. Gopalakrishnan, G. Madhusudan, and R.S. Tripathi, Optimization of Positioning of an Acoustic Emission Sensor for Monitoring Hot Forging, *Mater. Manuf. Process.*, 2006, **21**(5), p 543–549
28. A. Patel, S. Das, and B.K. Prasad, Hot Deformation Behaviour of AA2014—10 wt.% SiC Composite, *Trans. Indian Inst. Met.*, 2014, **67**(4), p 521–530
29. A. Patel, S. Das, A. Patel, and A.K. Bhattacharya, Microstructure and Crystallographic Texture of Aluminium Composite, *Chem. Mater. Res.*, 2013, **3**(11), p 25–27
30. K.N. Subramanium, T.R. Bieler, and J.P. Lucas, Mechanical Shaping of Metal Matrix Composites, *Key Eng. Mater.*, 1995, **104-107**, p 175–214
31. I. Ozdemir, U. Cocen, and K. Onel, The Effect of Forging on the Properties of Particulate-SiC-Reinforced Aluminium Alloy Composites, *Compos. Sci. Technol.*, 2000, **60**(3), p 411–419
32. F. Ma, S. Lu, P. Liu, W. Lu, and D. Zhang, Microstructure and Mechanical Properties Variation of TiB/Ti Matrix Composite by Thermo-mechanical Processing in Beta Phase Field, *J. Alloys Compd.*, 2017, **695**, p 1515–1522
33. F. Ma, P. Liu, W. Li, X. Liu, X. Chen, K. Zhang, D. Pan, and W. Lu, The Mechanical Behavior Dependence on the TiB Whisker Realignment During Hot-Working in Titanium Matrix Composites, *Sci. Rep.*, 2016, **6**, p 36126
34. R.D. Schuller and F.E. Wawner, Analysis of High Temperature Behaviour of AA2124/SiC Whisker Composites, *Compos. Sci. Technol.*, 1991, **40**(2), p 213–223
35. L. Ceshini, I. Boromei, G. Minak, A. Morri, and F. Tarterini, Microstructure, Tensile and Fatigue Properties of AA6061/20 vol.% Al_2O_3 Friction Stir Welded Joints, *Compos. Part A*, 2007, **38**(4), p 1200–1210
36. T.S. Srivatsan and A. Prakash, The Quasi-Static Fracture Behaviour of an Aluminium Alloy Metal Matrix Composites, *Compos. Sci. Technol.*, 1995, **54**(3), p 307–315